COBEM UBERLÂNDIA 2019

ABCM Associação Brasileira de Engenharia e Ciências Mecânicas

25th ABCM International Congress of Mechanical Engineering
October 20-25, 2019, Uberlândia, MG, Brazil

ACTIVE CONTROL OF BAND GAPS ON A SMART PHONONIC BEAM

Massao Kodama Dourado
Paulo José Paupitz Gonçalves
State University of São Paulo - UNESP, School of Engineering, Bauru Av. Eng. Luiz Edmundo C. Coube 14-01 - Bauru, SP - Brazil
m.dourado@unesp.br
paulo.jpg@feb.unesp.br

Carlos De Marqui Junior
Danilo Beli
Universidade de São Paulo - USP, Escola de Engenharia de São Carlos, Departamento de Engenharia Aeronáutica, Avenida Trabalhador São-Carlense 400, Pq. Arnold Schimidt - São Carlos, SP - Brazil
demarqui@sc.usp.br
dbeli@usp.br, beli.danilo@gmail.com

Abstract. *Periodic structures are systems composed of repeated fundamental blocks called unit cells. As well established in photonics and phononics or structural dynamics, these periodic structures present pass bands and stop bands, which are frequency ranges where waves can or cannot propagate, respectively. In phononic crystals, the frequency where a stop band occurs is defined by the geometric and material properties of the primary unit cell. With the objective of improving these passive characteristics, this paper investigates the influence of active control using piezoelectric elements as actuators. The passive and active structural influence of the piezoelectric elements coupled to a beam are investigated and their effects over the pass and stop bands are discussed. The electromechanical periodic system is modeled using the spectral element method.*

Keywords: *periodic structure, phononic crystals, smart materials, vibration attenuation, spectral elements*

1. INTRODUCTION

Periodic structures such as phononic crystals and metamaterials can be used as vibration filters or attenuators as well as to wave manipulation (Deymier (2013); Hussein *et al.* (2014)) due to the appearance of stop bands, also called band gaps, produced by Bragg scattering and local resonance phenomena. The Bragg scattering studied by Gupta (1970); Sigalas and Economou (1992); Mead (1996); Policarpo *et al.* (2010); Olhoff *et al.* (2012), among others, occurs due to the reflection of waves in the discontinuities between different materials or geometry placed periodically along the structure, reducing wave propagation in the structure for determined frequency intervals. The use of active control can lead to enhanced performance by extending these band gaps depending on the control approach used (Li *et al.*, 2017).

In the literature, many models were developed for the study of smart periodic structures. Thorp *et al.* (2001) developed a model for control of longitudinal wave propagation on rods with shunted periodically placed piezoelectric patches. Jang *et al.* (2014) proposed a fully coupled smart beam based on Timoshenko beam and Midlin-Herrmann rod theory. Cunha *et al.* (2016) studied the influence of uncertainties in the manufacturing parameters of beams in a smart lattice structure and their effects on the stop bands. Li *et al.* (2017) proposed the use of negative proportional feedback strategy for active control of a beam with periodically placed piezoelectric elements, which prevents instability on the active control. Li also verified the effects of tuning this control strategy in the dynamic response of the beam.

Several methods have been employed to investigate periodic structures. The Spectral Element Method (SEM), which is an analytic method in frequency domain used to obtain the wavenumbers and the forced response by using a dynamic stiffness matrix (Doyle (1997); Lee *et al.* (2000); Wu *et al.* (2014)). However, differently from the Finite Elements Method (FEM), the SEM is usually employed to simple one-dimensional systems such as rods, ducts, beams and Levy plates, which present closed-form solutions for the equations of motion (Doyle (1997); Lee (2009)). The SEM is significantly faster than the FEM due to its capacity to obtain accurate frequency responses from a uniform structure with a single element, as long as there are no discontinuities on it. This feature leads to a significantly smaller system to be solved, especially on high frequencies, in which FEM requires a high number of elements in order to appropriately describe the dynamic behavior of the system. On the other hand, as SEM is also an element method, if the studied system does present discontinuities on it, adequate mesh refining can be used in order to accurately describe the system.

The SEM approach consists in converting the partial differential equations of motion from time to frequency domain by application of the Discrete Fourier Transform (DFT). The system dynamic responses is then assumed to be a superposition

of a finite number of wave modes. The solutions of the discrete frequency equations results in the exact wave solutions, which are responsible for the frequency response precision of this method. The exact wave solutions are then derived, awarding the dynamic shape functions. From the dynamic shape functions, the dynamic stiffness matrix, also called spectral matrix, can be obtained. The spectral matrix of each element can then be assembled in the same manner as the conventional FEM, which leads to convenient modeling of periodic beams, as each uniform section can be represented by a single element.

The present work implements a spectral elements model for smart periodic beams. First, the effects of multiple piezoelectric elements (passive structural elements) periodically distributed along a free-free Euler-Bernoulli beam are discussed. Later, the effects of different feedback control approaches using the piezoelectric elements as actuators on the behavior of the periodic system are investigated.

2. MATHEMATICAL MODELING

2.1 Electromechanically coupled Beam

The unit cell considered in this work is based on two beam element models which are shown in Fig. 1. The system on the left hand side represents the SE element of an Euler-Bernoulli beam, with longitudinal and bending vibration modeled by the indicated degrees of freedom. The system on the right hand side represents the SE element beam with an additional piezoelectric layer.

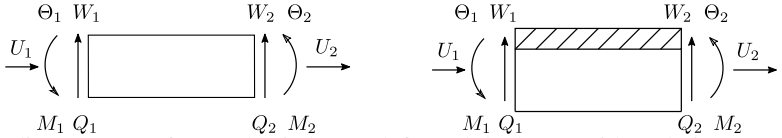

Figure 1: The coordinate system for an elastic beam (left) and the beam with and piezo patch attached (right)

For brevity, only the modeling procedure of the electromechanically coupled beam is described in this work, since the elementary Euler-Bernoulli beam model can be easily found in the literature (Doyle (1997); Lee (2009)). The electromechanically coupled beam is modeled assuming a bilayer cross section, such that the equivalent properties are defined as

$$EA = E_bA_b + E_pA_p, \qquad EI = E_bI_b + C_{11}^D I_p + (1/4)E_pA_ph^2, \qquad \rho A = \rho_bA_b + \rho_pA_p \tag{1}$$
$$\alpha = (1/2)\rho_pA_ph, \qquad \beta = (1/2)E_pA_ph, \qquad \gamma = (1/4)\rho_pA_ph^2$$

where, the subscripts b and p are related to the elastic beam and piezoelectric element properties. In addition, E is the material Young's modulus, ρ is the mass density, A is the cross section area, I is the second moment of area, h is the total thickness ($h = h_b + h_p$), C_{11}^D is the piezo elastic stiffness. The equations of motion are given by Lee *et al.* (2000)

$$EI\,w'''' + \rho A\,\ddot{w} + \alpha\,\ddot{u}_b' + \beta u''' + \gamma\ddot{w}'' = \quad p(x,t) \tag{2}$$
$$EA\,u_b'' - \rho A\,\ddot{u}_b + \alpha\,\ddot{w}' + \beta w''' = -\tau(x,t) \tag{3}$$

where $p(x,t)$ and $\tau(x,t)$ are external loadings. Assuming harmonic motion in the form, $w(x,t) = W(x)\mathrm{e}^{i\omega t}$ and $u(x,t) = U(x)\mathrm{e}^{i\omega t}$, the equations of motion are converted from space-time to space-frequency domain

$$EI\,W'''' - \omega^2\rho AW - \omega^2\alpha U' - \beta U''' + \omega^2\gamma W'' = P(x) \tag{4}$$
$$EA\,U'' + \omega^2\rho AU - \omega^2\alpha W' - \beta W''' = T(x) \tag{5}$$

and considering the case of free motion, the spatial solution is assumed in the spectral form as

$$W(x) = C\,\mathrm{e}^{-ikx}, \quad U(x) = r\,C\,\mathrm{e}^{-ikx}, \tag{6}$$

where C is the wave amplitude and r is the ratio between longitudinal and bending wave amplitudes. Moreover, Eq. 6 transforms the physical space x in the reciprocal space represented by the wavenumber k. Substituting Eq. 6 in the Eqs. (4-5), leads to

$$\begin{bmatrix} k^4\,EI - \omega^2\left(\gamma k^2 + \rho A\right) & ik\left(\alpha\omega^2 - \beta k^2\right) \\ ik\left(\alpha\omega^2 - \beta k^2\right) & \omega^2\rho A - k^2\,EA \end{bmatrix} \begin{bmatrix} 1 \\ r \end{bmatrix} = \begin{bmatrix} 0 \\ 0 \end{bmatrix} \tag{7}$$

and the determinant of Eq. 7 provides the dispersion equation or the dispersion relation $k(\omega)$

$$a_6k^6 + a_4k^4 + a_2k^2 + a_0 = 0 \tag{8}$$

where

$$a_6 = \beta^2 - EA\,EI; \qquad a_4 = \omega^2\left(EA\,\gamma + EI\,\rho A - 2\alpha\beta\right)$$
$$a_2 = -\omega^2\,\left(\omega^2\rho A\gamma - EA\rho A - \omega^2\alpha 2\right);\; a_0 = -\omega^4\rho A^2$$

The solution of Eq. 8 provides six roots or wavenumbers k_j, $j = 1, \cdots, 6$. In addition, the amplitude rations r_j are computed using Eq. 7 as

$$r_j = \frac{ik_j\left(\alpha\omega^2 - \beta k_j^2\right)}{\omega^2\rho A - k_j^2 EA}, \;\text{ for } j = 1, \cdots, 6 \tag{9}$$

By using the wavenumbers and the wave amplitude ratios, the spectral element matrix, also know as spectral dynamic stiffness matrix, of the electromechanically coupled beam $\mathbf{S}_p(\omega)$ is calculated following the procedure described in Lee *et al.* (2000) as

$$\mathbf{S}_p(\omega) = \mathbf{H}(\omega)^{-T}\mathbf{D}(\omega)\mathbf{H}(\omega)^{-1} \tag{10}$$

where

$$\mathbf{H}(\omega) = \begin{bmatrix} r_1 & r_2 & r_3 & r_4 & r_5 & r_6 \\ 1 & 2 & 3 & 4 & 5 & 6 \\ -ik_1 & -ik_2 & -ik_3 & -ik_4 & -ik_5 & -ik_6 \\ r_1\mathrm{e}_1 & r_2\mathrm{e}_2 & r_3\mathrm{e}_3 & r_4\mathrm{e}_4 & r_5\mathrm{e}_5 & r_6\mathrm{e}_6 \\ \mathrm{e}_1 & \mathrm{e}_2 & \mathrm{e}_3 & \mathrm{e}_4 & \mathrm{e}_5 & \mathrm{e}_6 \\ -ik_1\mathrm{e}_1 & -ik_2\mathrm{e}_2 & -ik_3\mathrm{e}_3 & -ik_4\mathrm{e}_4 & -ik_5\mathrm{e}_5 & -ik_6\mathrm{e}_6 \end{bmatrix} \tag{11}$$

where, $\mathrm{e}_j = \mathrm{e}^{ik_j L}$, and

$$\begin{aligned}\mathbf{D}(\omega) = &-EA\,\mathbf{RKEKR} + EI\,\mathbf{K}^2\mathbf{EK}^2 - i\beta\left(\mathbf{K}^2\mathbf{EKR} + \mathbf{RKEK}^2\right) \\ &-\omega^2\left[\rho A\left(\mathbf{E} + \mathbf{RER} + i\alpha\left(\mathbf{KER} + \mathbf{REK}\right) - \gamma\,\mathbf{KEK}\right]\end{aligned} \tag{12}$$

where $\mathbf{K} = \mathrm{diag}[k_j]$, $\mathbf{R} = \mathrm{diag}[r_j]$ and the elements of the matrix $\mathbf{E} = [E_{pq}]$ are calculated as

$$E_{pq} = \begin{cases} \dfrac{i\left(\mathrm{e}^{-i(k_p+k_q)L} - 1\right)}{k_p + k_q}, & \text{if } k_p + k_q \neq 0 \qquad (p, q = 1, 2\cdots 6) \\ L, & \text{if } k_p + k_q = 0 \end{cases} \tag{13}$$

and the spectral element equation is given as

$$\mathbf{f}(\omega) = \mathbf{S}(\omega)\mathbf{d} \quad \text{or} \quad \mathbf{d}(\omega) = \mathbf{R}(\omega)\mathbf{f}, \quad \mathbf{R} = \mathbf{S}^{-1} \tag{14}$$

where $\mathbf{f}$ is the external forces vector and $\mathbf{d}$ is the degrees of freedom vector in the form

$$\mathbf{f} = \{N_1 \quad Q_1 \quad M_1 \quad N_2 \quad Q_2 \quad M_2\}^T \quad \text{and} \quad \mathbf{d} = \{U_1 \quad W_1 \quad \Theta_1 \quad U_2 \quad W_2 \quad \Theta_2\}^T$$

2.2 Piezoelectric Feedback Control

This section presents the development of three different active feedback control strategies to minimize the vibration levels of the periodic electromechanically coupled beam. These strategies are based on local control, minimizing the vibration levels of each cell individually. Fig. 2 shows the control configuration for a cell with a piezoelectric element. The transverse displacement W_2 (right end) is used as the feedback signal, indicated by the sensor. In the case of using an accelerometer, the displacement signal may be obtained by integrating twice this signal in the time domain. When voltage is applied to the piezoelectric actuator, it produces control forces and moments given as

$$\mathbf{f_c} = \left\{ \; -N_c \quad 0 \quad M_c \quad N_c \quad 0 \quad -M_c \; \right\}^T$$

This way, the displacements can be calculated considering the external forces ($\mathbf{f}$) and control forces ($\mathbf{f}_c$) using Eq. 14 as

$$\mathbf{d} = \mathbf{R}(\mathbf{f} + \mathbf{f}_c) \tag{15}$$

In the feedback control case, the control forces ($\mathbf{f}_c$) can be written as a function of the displacement as

$$\mathbf{d} = \mathbf{R}(\mathbf{f} + \mathbf{H}_c\mathbf{d}) \tag{16}$$

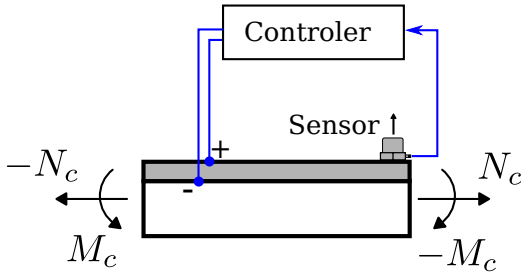

Figure 2: Schematic configuration of feedback control strategy of each individual cell.

where the control matrix $\mathbf{H}_c$ takes into account the feedback signal W_2 and can be written as

$$\mathbf{H}_c = \begin{bmatrix} 0 & 0 & 0 & 0 & -\sigma_1 & 0 \\ 0 & 0 & 0 & 0 & 0 & 0 \\ 0 & 0 & 0 & 0 & \sigma_2 & 0 \\ 0 & 0 & 0 & 0 & \sigma_1 & 0 \\ 0 & 0 & 0 & 0 & 0 & 0 \\ 0 & 0 & 0 & 0 & -\sigma_2 & 0 \end{bmatrix} \tag{17}$$

in which σ_1 and σ_2 depend on the piezoelectric material properties as

$$\sigma_1 = bd_{31}E_pH, \quad \sigma_2 = \frac{1}{2}bd_{31}E_phH \tag{18}$$

In which d_{31} is the piezoelectric constant, and H is the control strategy. In this paper, the three different control strategies employed are defined as

$$H_d = K_d, \quad H_v = K_v j\omega, \quad H_a = -K_a\omega^2 \tag{19}$$

where, K is the feedback control gain and the subscripts d, v and a relate to the displacement, velocity and acceleration relative gains, respectively. Rearranging Eq. 16, it is possible to obtain the closed loop receptance matrix as

$$\mathbf{d} = \mathbf{R}_{cl}\mathbf{f} \tag{20}$$

where

$$\mathbf{R}_{cl} = [\mathbf{I} - \mathbf{R}\mathbf{H}_c]^{-1}\,\mathbf{R} \tag{21}$$

and the spectral element matrix in closed loop is

$$\mathbf{S}_{cl} = \mathbf{R}_{cl}^{-1} \tag{22}$$

Finally, after the assembling procedure and by imposing adequate boundary conditions, the spectral global equation is given by

$$\mathbf{f}_g(\omega) = \mathbf{S}_g(\omega)\mathbf{d}_g(\omega) \tag{23}$$

where $\mathbf{f}_g$ is the global forces vector, $\mathbf{S}_g$ is the global stiffness matrix and $\mathbf{d}_g$ is the global degrees of freedom vector.

2.3 Wave Propagation Analysis

Let $\mathbf{T}$ be the transfer matrix of a single cell and λ its eigenvalues. The propagating wave phase (ϵ) and attenuation (μ) are given by

$$\epsilon = Re(ln(\lambda)/\sqrt{-1}), \quad \mu = Im(ln(\lambda)/\sqrt{-1}) \tag{24}$$

2.4 Stability analysis

The use of active control raises concerns regarding control stability since external energy is supplied to the system (Huang *et al.*, 2003). Therefore, before application of the active control, the feedback control must be proven to be stable.

In order to prove the control stability, let $\mathbf{L} = \mathbf{R}\mathbf{H_c}$ be the open loop transfer matrix. The generalized Nyquist theorem (Skogestad and Postlethwaite, 2005) states that the controlled system is stable if, and only if the Nyquist plot of $det(\mathbf{I}+\mathbf{L})$ does not encircles the origin as will be discussed in section 3.3 of this paper.

Base beam			Piezoelectric element		
l_b	0.200	m	l_p	0.100	m
b_b	0.010	m	b_p	0.010	m
h_b	0.005	m	h_p	0.001	m
ρ_b	1140	kg/m^3	ρ_p	7800	kg/m^3
E_b	$3.5 \cdot 10^9(1+i\eta)$	Pa	E_p	$75 \cdot 10^9$	Pa
η	0.005		C_{11}^D	$75 \cdot 10^9$	Pa
			d_{31}	$-1.75 \cdot 10^{-10}$	m/V

Table 1: Material properties for base beam and piezoelectric element

3. RESULTS AND DISCUSSION

3.1 Passive Response

The investigation in this paper considers the electromechanical phononic crystal shown in Fig. 3, which consists of a beam with periodically placed piezoelectric elements, each one with an ideal controller and a massless sensor.

As spectral elements can be assembled in the same manner as finite elements, as mentioned previously, each cell (Fig. 3) will be added to the end of the previous cell, sharing the same forces and displacements on shared nodes. The numerical simulations consider the properties values given in Tab. 1 for a nylon base beam with a PZT piezoelectric element.

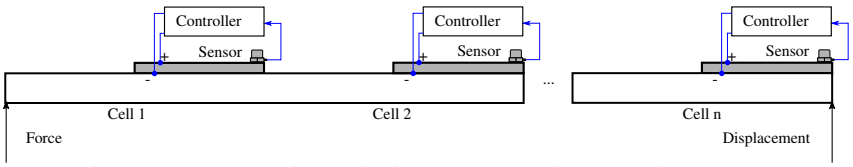

Figure 3: A beam with periodically spaced piezoelectric elements

In order to investigate the structural influence of the periodic piezoelectric elements on the base beam system, considered in this case as passive structural elements, a comparison between a system with 1, 5 and 10 periodic cells was simulated. The dynamic response is computed considering an unitary vertical harmonic force applied at the left side of the beam ($Q_1^{\texttt{cell 1}} = 1$), the vertical displacement is measured at the right side the beam ($W_2^{\texttt{cell n}}$), as shown in the Fig. 3.

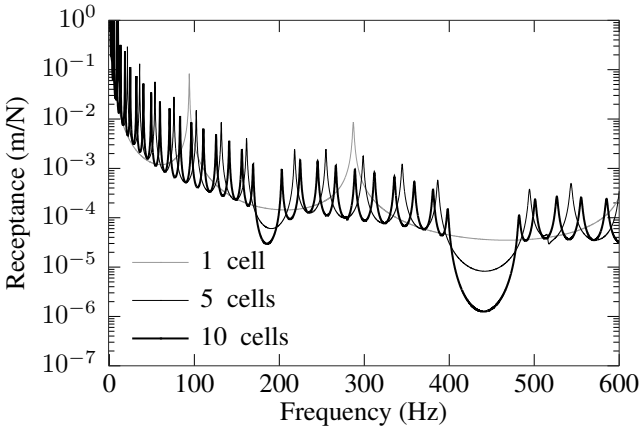

Figure 4: Comparison of the periodic beam frequency response with different number of cells

Fig. 4 shows the influence of increasing the number of cells in the dynamic response of the periodic beam. Due to the higher number of cells, the wave reflection on each discontinuity greatly inhibits wave propagation along the beam for some frequency intervals. In the case studied, three band gaps are present in the 0-600Hz interval, being the first a small band gap between 44 to 46 Hz, the second between 173 to 219 Hz and the third in the 405 to 474 Hz band.

3.2 Active Control

Three active control approaches discussed in section 2.2, were applied to the electromechanical phononic beam with 10 unit cells.

Firstly, arbitrary gains were tested in order to check the influence of the piezoelectric active control strategies on the general frequency response. The applied external force and the measured displacement were obtained in the same manner as described in the passive response evaluation of the system, with results shown in Fig. 5. Fig. 5(a) shows the effect of increasing the displacement proportional gain. The attenuation of the small band gap between 44 to 46 Hz, increases with increasing gain value. The effect of velocity proportional gain increase are displayed in Fig. 5(b). The peak values are reduced due to enhanced damping related to velocity feedback. Moreover, the bandwidth of band gaps as well as the lower attenuation are slightly reduced, which is a generally unwanted effect for periodic structures. Fig. 5(c) shows that an increase in acceleration related gain results in a wider and more attenuated band gap between 400 and 500 Hz, with little effect over lower frequencies.

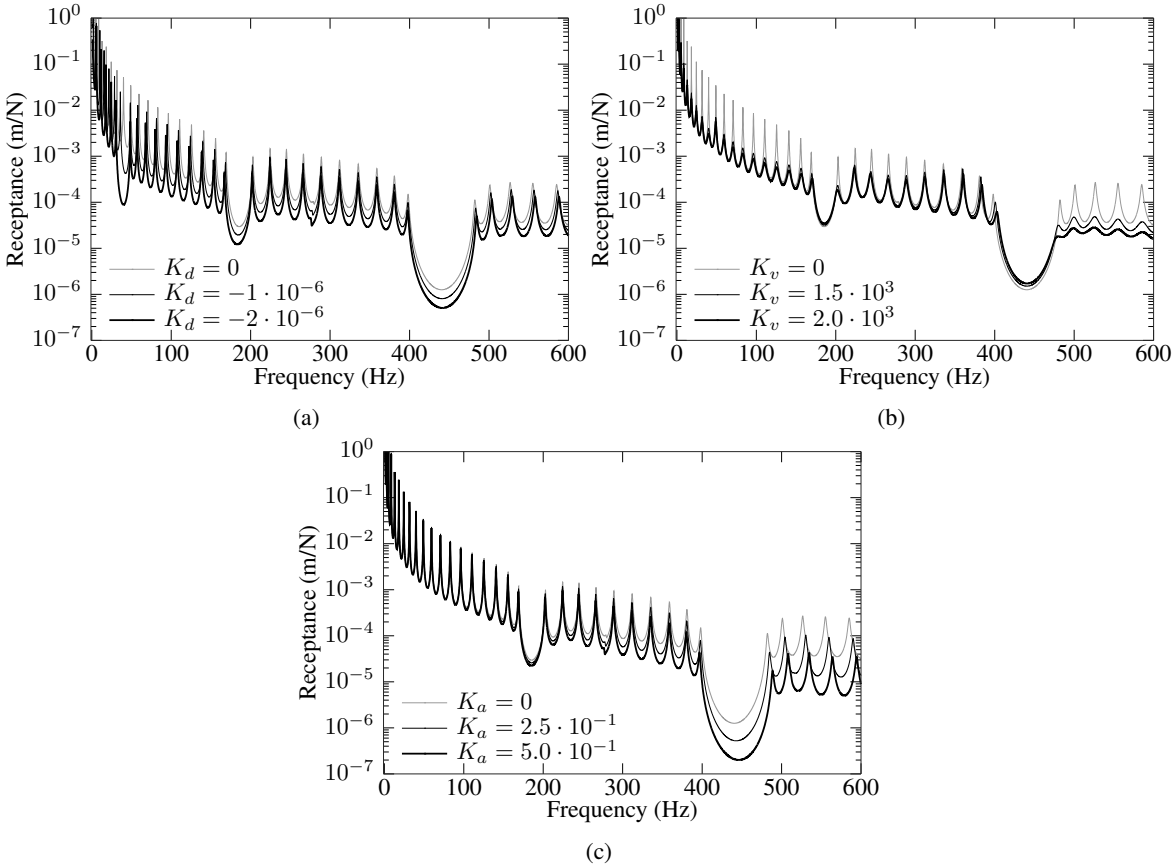

Figure 5: Influence of gain increase on: (a) displacement proportional gain, (b) velocity proportional gain and (c) acceleration proportional gain

It is worthy noticing that no physical constrain was defined for the gains chosen in Fig. 5, as their goal was to verify the possible effects of gain increases on the stop bands of the phononic beam, in the selected frequency interval. Thus, control gain values K_d, K_v and K_a were selected in order to ensure that the longitudinal forces exerted by the piezoelectric elements would be 100 N at most, in a range 5Hz away from the extremities of the later two passive band gaps (168 to 479 Hz), for each control approach. The resulting frequency response plots can be seen in Figs. 6 and 7.

Figs. 8(a), 9(a) and 10(a) show the comparison between the frequency response of the passive and active beam , for the different control approaches, respectively. Figs. 8(b), 9(b) and 10(b) show the values of wave phase (ϵ) and attenuation (μ) on the same ordinate axis, for easier visualization. Gray lines refer to the passive response of the system, while black lines refer to the different control approaches.

A direct comparison between the studied control approaches can be seen in Figs. 6 and 7. It is shown that both the displacement and acceleration proportional feedback improve the beam band gap sizes while also reducing the vibration amplitude in the band gap, being that the acceleration feedback approach shows the best results among the three, for this frequency interval. The velocity proportional feedback approach did the opposite for the third band gap, as the increased damping of the system results in worse attenuation at higher frequencies.

The control efforts applied in each case at the first cell are shown in Fig. 11. Filled lines represent the longitudinal

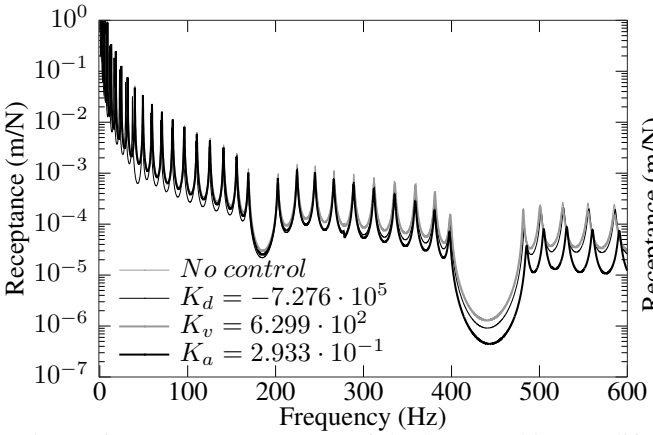

Figure 6: Frequency response of the beam, subject to different control approaches

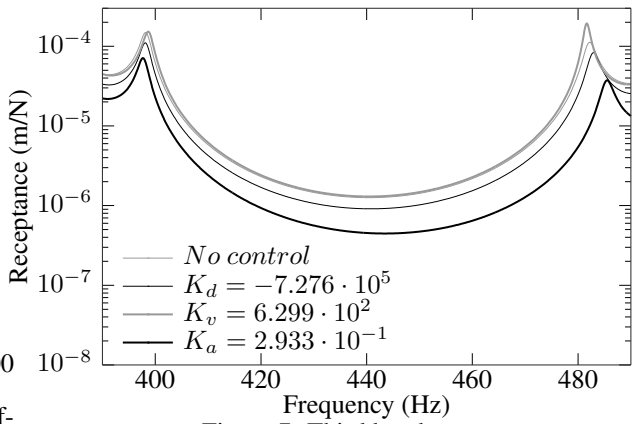

Figure 7: Third band gap

control forces (N), while dashed lines represent the control moments (M), in Newton and Newton.meter, respectively. The subscripts d, v and a refer to displacement, velocity and acceleration control gains, respectively. For each following unit cell, control forces are shown to be lower inside the band gap interval. The overall behavior of the control forces for each cell is illustrated on Fig. 12 for the displacement proportional feedback. For other control approaches, the results are not shown, but the behavior in the stop bands frequencies is similar.

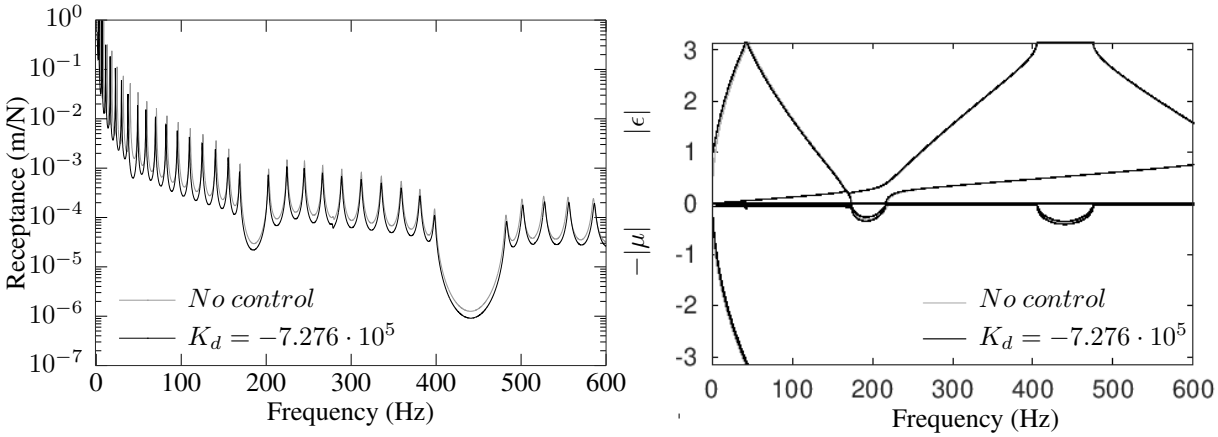

(a) (b)

Figure 8: (a) Frequency response and (b) wave propagation plots for displacement proportional feedback

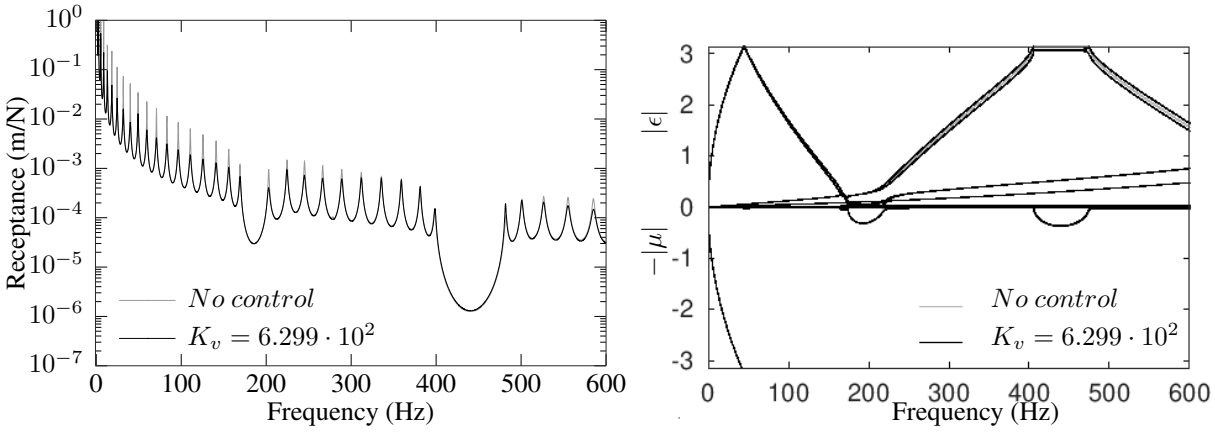

(a) (b)

Figure 9: (a) Frequency response and (b) wave propagation plots for velocity proportional feedback

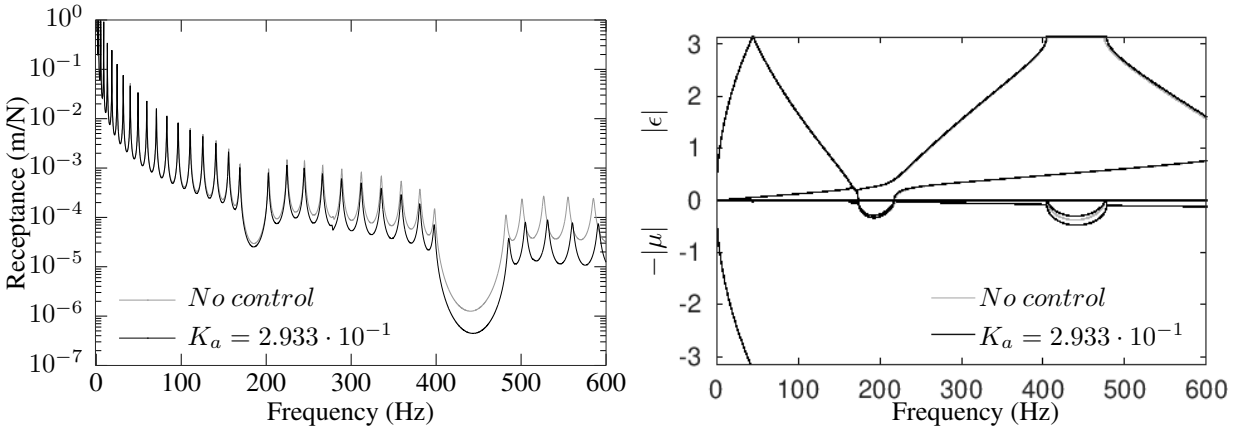

(a) (b)

Figure 10: (a) Frequency response and (b) wave propagation plots for acceleration proportional feedback

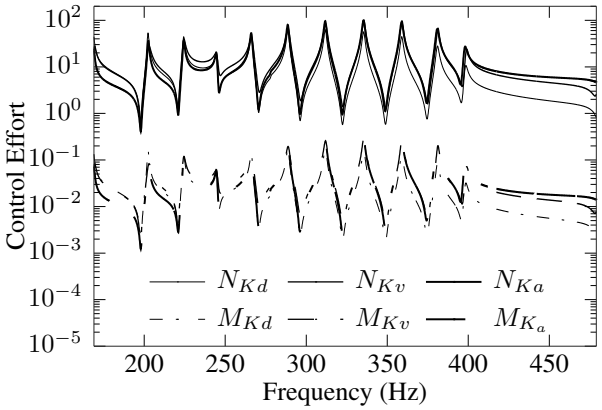

Figure 11: Control efforts applied on the first cell, for each control strategy

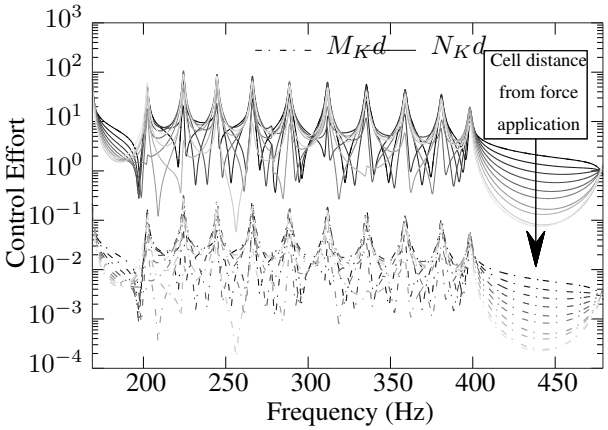

Figure 12: Applied force variation per cell, for displacement proportional feedback

In the control force plots, specially in the band gap frequencies, the force needed to control each subsequent cell is lower than the previous, which may be exploited in order to achieve better vibrational insulation on desired frequencies.

3.3 Stability Assessment

The Nyquist plots regarding the system control are plotted in Figs. 13 to 15. It was verified that, for the frequency interval from 0 Hz to 10000 Hz, there was no encirclement of the origin. Therefore, for the three control strategies applied, no control induced instability is expected in the frequency range used in the examples.

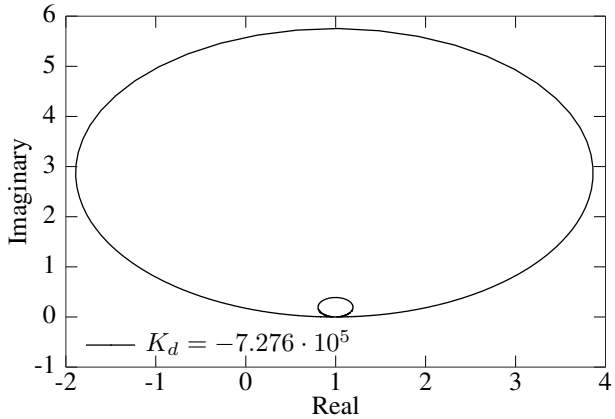

Figure 13: Nyquist plot of the displacement proportional feedback

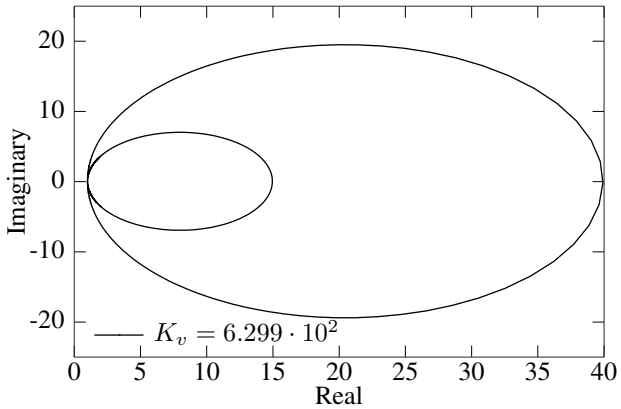

Figure 14: Nyquist plot of the velocity proportional feedback

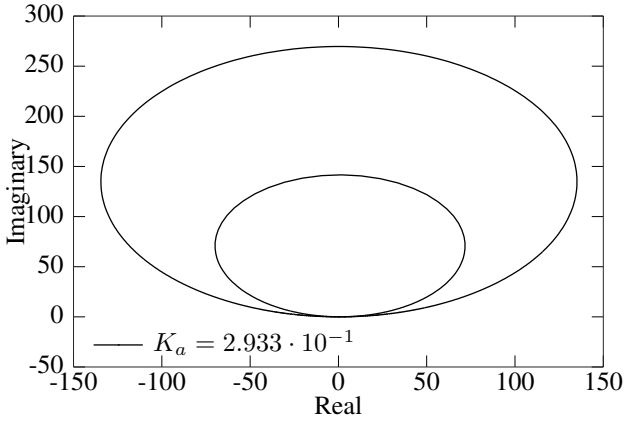

Figure 15: Nyquist plot of the acceleration proportional feedback

4. CONCLUSIONS

The geometric and material periodicity created by the addition of piezoelectric elements produced an electromechanical phononic structure, which induced Bragg scattering band gaps. This result, although not unprecedented, indicates the viability of spectral modeling for analysis of band gaps in smart structures.

Using the model presented for active control of the piezoelectric element, it was verified that different control strategies can change the bandwidth and intensity of the band gaps. Control gains could also be defined in order to meet a specified load exerted by the piezoelectric element, which, although may be excessive for the case studied, could be of interest for vibration suppression in lower input loads, which would result in lower forces being applied by the piezoelectric element. It was also verified that control forces required to suppress vibrations are reduced for each successive unit cell, specially in the band gap areas, which leaves room for further improvement of control approaches, such as tuning the gains for each cell individually, in order to improve the suppression effects of the structural band gaps along with the chosen control approach.

Regarding the different control approaches, the acceleration relative feedback gain showed the best performance among the three, specially in the third band gap region, in which both the band gap size increased and the receptance of the beam decreased with a higher intensity than the others. The three control approaches tested were also verified to be stable at the frequency interval being studied.

As a main conclusion, the feedback control of smart phononic beams was shown to be an alternative to tune band gaps bandwidth, although further research on the optimal parameters for control may be needed in order to produce results involving larger increases on band gaps sizes.

5. ACKNOWLEDGEMENTS

D. Beli and C. De Marqui Jr. would like to thank the São Paulo Research Foundation (FAPESP - São Paulo, Brazil), through project number 2018/18774-6 and 2018/15894-0 for the financial support.

6. REFERENCES

Cunha, L., Ouisse, M. and Rade, D., 2016. "Robust smart periodic truss". In *Proceedings of ISMA 2016*, p. 14.

Deymier, P.A., 2013. *Acoustic Metamaterials and Phononic Crystals*. Springer Series in Solid-State Sciences 173. Springer, New York. doi:10.1007/978-3-642-31232-8.

Doyle, J., 1997. *Wave Propagation in Structures: Spectral Analysis Using Fast Discrete Fourier Transforms*. Mechanical Engineering Series. Springer New York. ISBN 9780387949406.

Gupta, G.S., 1970. "Natural flexural waves and the normal modes of periodically-supported beams and plates". *Journal of Sound and Vibration*, Vol. 13, No. 1, pp. 89 – 101.

Huang, X., Elliott, S. and Brennan, M., 2003. "Active isolation of a flexible structure from base vibration". *Journal of Sound and Vibration*, Vol. 263, pp. 357–376. doi:10.1016/S0022-460X(02)01057-X.

Hussein, M.I., Leamy, M.J. and Ruzzene, M., 2014. "Dynamics of phononic materials and structures: Historical origins, recent progress, and future outlook". *Applied Mechanics Reviews*, Vol. 66, No. 4, pp. 040802–040802–38. doi: 10.1115/1.4026911.

Jang, I., Park, I. and Lee, U., 2014. "Spectral element modeling and analysis of the dynamics and guided waves in a smart beam with a surface-bonded pzt layer". *Journal of Mechanical Science and Technology*, Vol. 28, No. 4, pp. 1229–1239.

Lee, U., 2009. *Spectral Element Method in Structural Dynamics*. Wiley. ISBN 9780470823750.

Lee, U., Kim, J. and Leung, A., 2000. "The spectral element method in structural dynamics". *The Shock and Vibration Digest*, Vol. 32, pp. 451–465.

Li, F., Zhang, C. and Liu, C., 2017. "Active tuning of vibration and wave propagation in elastic beams with periodically placed piezoelectric actuator/sensor pairs". *Journal of Sound and Vibration*, Vol. 393, pp. 14 – 29.

Mead, D., 1996. "Wave propagation in continuous periodic structures: Research contributions from southampton, 1964–1995". *Journal of Sound and Vibration*, Vol. 190, No. 3, pp. 495 – 524.

Olhoff, N., Niu, B. and Cheng, G., 2012. "Optimum design of band-gap beam structures". *International Journal of Solids and Structures*, Vol. 49, No. 22, pp. 3158 – 3169.

Policarpo, H., Neves, M. and Ribeiro, A., 2010. "Dynamical response of a multi-laminated periodic bar: Analytical, numerical and experimental study." *Shock & Vibration*, Vol. 17, No. 4/5, pp. 521 – 535. ISSN 10709622.

Sigalas, M. and Economou, E., 1992. "Elastic and acoustic wave band structure". *Journal of Sound and Vibration*, Vol. 158, No. 2, pp. 377 – 382. ISSN 0022-460X. doi:10.1016/0022-460X(92)90059-7.

Skogestad, S. and Postlethwaite, I., 2005. *Multivariable Feedback Control: Analysis and Design*. John Wiley & Sons, Inc., USA. ISBN 0470011688.

Thorp, O., Ruzzene, M. and Baz, A., 2001. "Attenuation and localization of wave propagation in rods with periodic shunted piezoelectric patches". *Smart Materials and Structures*, Vol. 10, No. 5, pp. 979–989.

Wu, Z.J., Li, F.M. and Wang, Y.Z., 2014. "Vibration band gap properties of periodic mindlin plate structure using the spectral element method". *Meccanica*, Vol. 49, No. 3, pp. 725–737.

7. RESPONSIBILITY NOTICE

The authors are the only responsible for the printed material included in this paper.